ACS OMEGA

Open Access

http://pubs.acs.org/journal/acsodf

Article

Gallic Acid-Modified Polyethylenimine−Polypropylene Carbonate−Polyethylenimine Nanoparticles: Synthesis, Characterization, and Anti-Periodontitis Evaluation

Zunxuan Xie, Boyang Gao, Jinyao Liu, Jiaming He, Yuyan Liu,* and Fengxiang Gao*

Cite This: *ACS Omega* 2024, 9, 14475−14488

Read Online

ACCESS | Metrics & More | Article Recommendations | Supporting Information

ABSTRACT: The aim of the research was to develop novel gallic acid (GA)-modified amphiphilic nanoparticles of polyethylenimine (PEI)−polypropylene carbonate (PPC)−PEI (PEPE) and comprehensively assess its properties as an antiperiodontitis nanoparticle targeting the Toll-like receptor (TLR). The first step is to evaluate the binding potential of GA to the core trigger receptors TLR2 and TLR4/MD2 for periodontitis using molecular docking techniques. Following this, we conducted NMR, transmission electron microscopy, and dynamic light scattering analyses on the synthesized PEPE nanoparticles. As the final step, we investigated the synthetic results and in vitro antiperiodontitis properties of GA-PEPE nanoparticles. The investigation revealed that GA exhibits potential for targeted binding to TLR2 and the TLR4/MD2 complex. Furthermore, we successfully developed 91.19 nm positively charged PEPE nanoparticles. Spectroscopic analysis indicated the successful synthesis of GA-modified PEPE. Additionally, CCK8 results demonstrated that GA modification significantly reduced the biotoxicity of PEPE. The in vitro antiperiodontitis properties assessment illustrated that 6.25 μM of GA-PEPE nanoparticles significantly reduced the expression of pro-inflammatory factors TNF-α, IL-1β, and IL-6. The GA-PEPE nanoparticles, with their targeted TLR binding capabilities, were found to possess excellent biocompatibility and antiperiodontitis properties. GA-PEPE nanoparticles will provide highly innovative input into the development of anti- periodontitis nanoparticles.

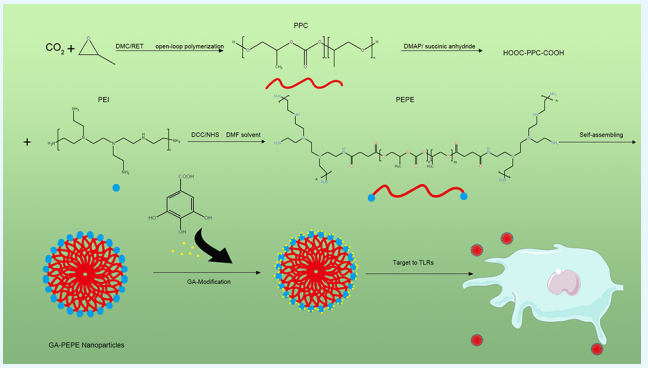

INTRODUCTION

Periodontitis is a chronic multifactorial inflammatory disease characterized by the progressive destruction of periodontal tissues, which greatly threatens people's health.[1,2] The membrane-bound toll-like receptors (TLRs) are a subset of the innate immune system's pattern recognition receptors (PRRs).[3] Among them, TLR2 identifies lipoproteins, while TLR4 recognizes lipopolysaccharides, both of which activate downstream NF-κB inflammatory pathways and the p38 mitogen-activated protein kinase (MPK) signaling pathway, contributing to the periodontitis and other inflammatory response.[4−7] The TLR4-MD2 complex is critical for recognizing LPS undergoing homodimerization as a key to exerting an innate immune response.[8] Correspondingly, targeted anti-inflammatory strategies against TLRs are essential for managing inflammation effectively.[9,10]

Nanoparticles loaded with drugs are at the forefront of research to enable anti-inflammatory strategies.[11−13] Polyethylenimine (PEI) is a hydrophilic polymer characterized by a linear or branched structure.[14] Due to its self-assembly behavior, PEI demonstrates significant potential for nanoparticle formation with various hydrophobic polymers, including poly(methyl methacrylate) (PMMA), poly(ε-caprolactone)-pluronic-poly-(ε-caprolactone) (PCFC), poly(caprolactone) (PCL), and poly(lactic acid) (PDL), and can even be combined with hydrophilic poly(ethylene glycol) (PEG) to form more complex nanoparticles.[15−19] PEI is extensively utilized in the synthesis of amphiphilic copolymers with hydrophobic polymers, leading to the formation of nanoparticles. Notably, nanoparticles derived from the hydrophobic polylactic acid-hydroxyacetic acid copolymer (PLGA)-PEI have exhibited promising applications in immunomodulation, siRNA delivery, DNA transfection, exosome delivery, and loading of tumor-targeting drugs.[20−23] This versatility is attributed to the high number of amino groups in PEI, which facilitates modifications. However, the highly positively charged structure of these amines renders cells more susceptible to damage, rendering PEI notoriously cyto-

Received: January 8, 2024
Revised: February 6, 2024
Accepted: March 1, 2024
Published: March 15, 2024

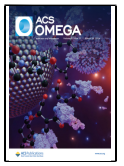

toxic.[24−27] As a result, reducing the cytotoxic effects of PEI is a primary consideration in the design of PEI nanoparticles.[24]

Poly(propylene carbonate) (PPC) is a biodegradable polymer that arises from the copolymerization of greenhouse gas CO2 and propylene oxide (PO).[28,29] The excellent biocompatibility properties of PPC can be attributed to its nontoxic, nonpolluting, and degradable nature.[30,31] As a result, PPC has found diverse applications in medicine delivery.[32,33] PPC is strongly hydrophobic[34] and the establishment of hydrophilic and hydrophobic self-assembled nanoparticles greatly extends the drug delivery application of PPC. Chitosan-PPC-based nanoparticles have demonstrated exceptional antimicrobial performance,[32] while self-assembling PPC nanoparticles have exhibited superior capability in delivering doxorubicin.[35]

Gallic acid is a naturally occurring polyphenolic compound known for its outstanding antioxidant and anti-inflammatory properties.[36−39] However, it suffers from rapid metabolism, low bioavailability, poor solubility, and instability. Consequently, nanoparticle delivery of gallic acid presents an opportunity to overcome these traditional pharmacokinetic challenges.[39−41]

Computer docking simulations have been widely used to analyze the targeting relationship between drugs and molecules Autodock software simulated the docking ability of peroxisome proliferator-activated receptor-γ with drug candidates, confirming the drug potential of plant-derived phenolics phloretin and phloridzin as insulin sensitization properties.[42] Meanwhile, the ability of drugs targeting mutant HER2 receptors was verified with the help of computer docking methods and potential drugs for malaria treatment were screened.[43,44] At a deeper level of molecular docking and molecular dynamics simulations, the conformational effects induced by antigenic mutations in the nucleus of proliferating cells and even the mechanisms that inhibit mismatch repair can be fully elaborated.[45,46] Most notably, the molecular dynamics perspective helps to understand the subsequent effects of mutations in important molecules, leading to the development of personalized targeted drugs.[47]

This study utilized a molecular docking method to assess the potential of GA to bind to TLR2/TLR4. Additionally, a novel GA-modified PEI−PPC-PEI (PEPE) amphiphilic nanoparticle was developed to facilitate a new delivery mode of GA. In this nanoparticle, PEI and PPC act as hydrophilic and hydrophobic chain segments, respectively. By modification of the amino group of the PEI segment with GA, the toxicity was reduced while achieving targeted binding for anti-inflammatory action. Notably, our study is the first to comprehensively characterize the physicochemical properties and antiperiodontitis effects of GA-PEPE nanoparticles, thereby providing a theoretical basis for the targeted anti-inflammatory treatment of pulpitis.

METHODS AND MATERIALS

Materials. Propylene oxide (PO) obtained from the Jilin Shenhua Group was dried under 3 Å molecular sieve until the water content was below 50 ppm. CO_2, sourced from Changchun Juyang Gas, had a water content below 50 ppm. Polyethylenimine (PEI) (Mw: 1800) was purchased from Kemike Biomedical Technology Co (Wuhan, China). Succinic anhydride, dicyclohexylcarbodiimide (DCC), 4-dimethylaminopyridine (DMAP), and *N*-hydroxy succinimide (NHS) were procured from Yuanye Bio-Technology Co (Shanghai, China). 99% purity Rhawn gallic acid (99% purity) was purchased from Yien Chemical Technology (Shanghai, China). Additionally, all solvents utilized in this study were obtained from the Institute of Applied Chemistry (Changchun, China). Vikase dialysis membranes with a molecular weight cut off (MWCO) of 8000−14000 and MWCO of 1000 were purchased from Rialai Biological Instrument consumables distributor (Beijing, China). All materials were used as received without further purification except for dialysis bags, which underwent appropriate pretreatment before use.

Molecular Docking between GA and Toll-Like Receptor (TLR). The molecular structures of gallic acid were obtained using PubChem (compound CID: 370), while the protein structures of the TLR2 (PDB ID: 1FYW) and TLR4/MD2 complex (PDB ID: 2Z64) were retrieved from the PDB database. The protein structure was then processed by using PyMOL to remove water molecules and ligands. Further processing of ligands and receptors, such as adding hydrogen atoms and determining active pockets, was carried out by using AutoDock Tools. The binding modes were analyzed using AutoDock4 software with "Genetic Algorithm" as the docking parameter. The 10 lowest binding energy modes were selected by the "ranked by energy" function of AutoDockTools. Finally, the model with the lowest binding free energy was selected, and PyMOL was used for providing visualization into the potential binding ability of gallic acid and TLR2/TLR4.

Synthesis of Polypropylene Carbonate (PPC). The PPC was synthesized through the utilization of a combinatorial catalyst system consisting of double metal cyanide catalyst (DMC) and colorless rare earth ternary (RET), as indicated in prior research.[48] The 200 mL portion of propylene oxide (PO) and the combinatorial catalyst were introduced into a 500 mL pretreated autoclave, ensuring the absence of oxygen and water. The copolymerization of carbon dioxide (CO_2) and PO was then initiated at 4 MPa and 70 °C. Following a 10 h reaction duration, the copolymerization process was halted by the addition of a methanol solution containing 5% dilute hydrochloric acid. The resulting white polymeric product (PPC) was subsequently subjected to drying at 40 °C under a vacuum until a constant weight was achieved.

Synthesis of HOOC−PPC−COOH. The reaction commenced with dissolving PPC (6.32 g, 0.0004 mol) in 100 mL of dichloromethane (DCM) followed by the addition of succinic anhydride (0.2 g, 0.002 mol) and 4-dimethylaminopyridine (0.244 g, 0.002 mol) to the solution. The reaction mixture was then subjected to 24 h at 40 °C under magnetic stirring. Subsequently, the product was precipitated with excess methanol and purified using a vacuum drying oven to remove the remaining solvent. This purification process was repeated three times to ensure purity of the products. Lastly, the products were utilized in determining the acid value by titration with potassium hydroxide ethanol.

Synthesis of Amphiphilic Polymer PEI−PPC−PEI. The synthesis of block copolymers began with the dissolution of 5.06 g (0.32 mmol) of HOOC-PPC−COOH in 100 mL of dimethylformamide (DMF), in accordance with previous research.[49] Dicyclohexylcarbodiimide (DCC) (263.7 mg, 1.28 mmol) and *N*-hydroxysuccinimide (NHS) (147.2 mg, 1.28 mmol) were added to the polymer solution and left to react under magnetic stirring for 24 h at room temperature. Following this, the polymer solution was introduced into polyethylenimine (PEI) (1.28 mmol) in DMF and allowed to react for another 24 h under magnetic stirring. The filtration process was used to remove insoluble dicyclohexylurea from the reaction mixture.

Also, polymer product was then isolated by precipitation into excess diethyl ether under vigorous stirring. Subsequently, the

https://doi.org/10.1021/acsomega.4c00261
ACS Omega 2024, 9, 14475−14488

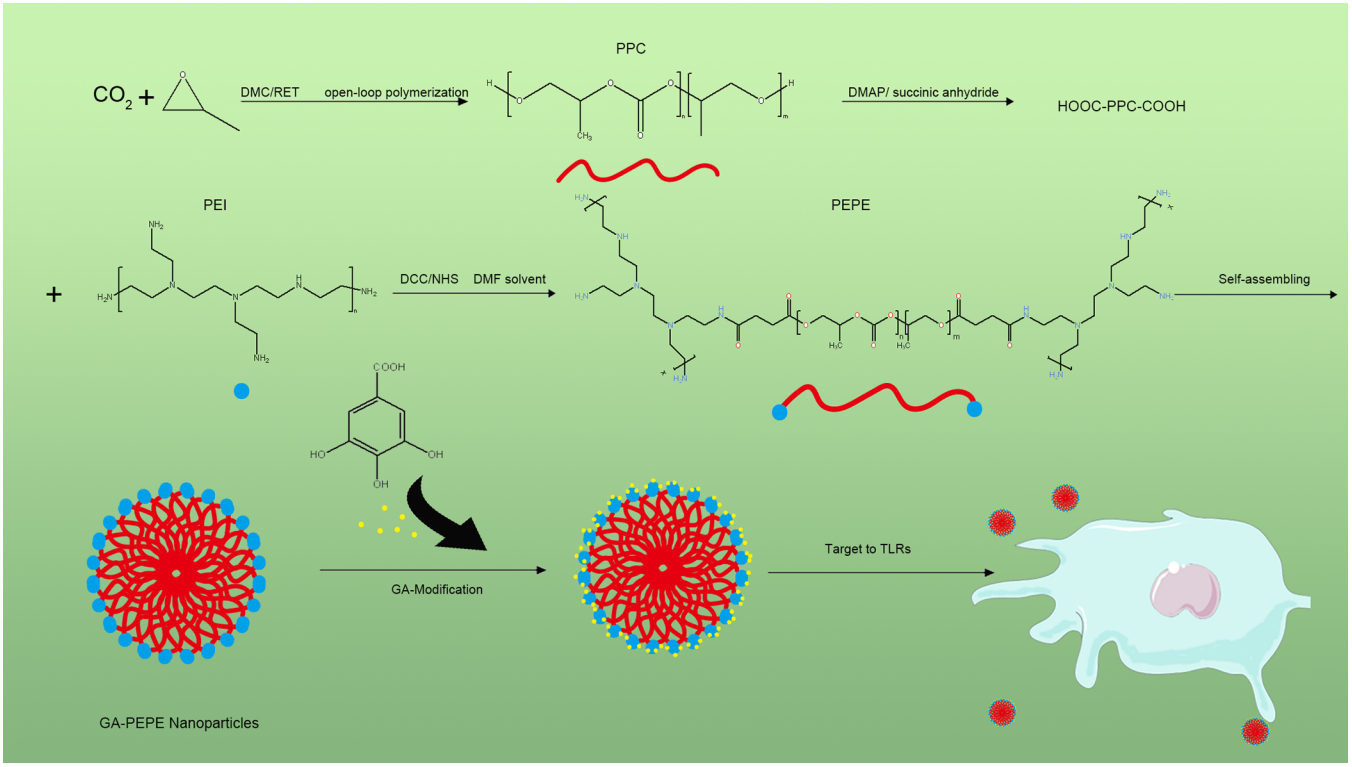

Figure 1. Scheme of the study.

product was dissolved in dimethyl sulfoxide (DMSO) and subjected to dialysis against excess deionized distilled water using a dialysis membrane (MWCO:8000−14000 DA). This purification procedure was repeated twice to ensure the removal of the impurities. The hydrogen spectra of the PEI−PPC−PEI copolymer were analyzed in $CDCl_3$ as a medium using AVANCE NEO 400 M HZ NMR (Bruker, Karlsruhe, German). Avance Neo parameters are provided in Table S1.

Preparation of PEI−PPC−PEI Nanoparticle Solution. The PEI−PPC-PEI nanoparticles were prepared by dissolving 100 mg (about 5 μmol) of PEI−PPC−PEI in 5 mL of DMF, followed by the dropwise addition of this mixture into 20 mL of PBS (pH 7.4, ServiceBio, Wuhan, China) under magnetic stirring. The resulting suspension was dialyzed in PBS for 24 h using a dialysis membrane (MWCO: 1000 DA) to achieve a nanoparticle concentration of 200 μM in the PBS solution.

Synthesis of Gallic Acid-Modified PEI−PPC−PEI Nanoparticles. Gallic acid-modified PEI−PPC−PEI (GA-PEPE) nanoparticles were prepared in a series of steps using a DMF-PBS system. First, 4 mL of DMF solution containing 100 mg of PEPE was added dropwise to 20 mL of PBS solution under swirling conditions to form PEPE nanoparticle DMF/PBS solution. Then, 1 mL of DMF containing 10 mg of gallic acid was added dropwise to the above PEPE nanoparticle DMF/PBS solution, and the resulting mixture was stirred for 24 h. This allowed the gallic acid to react with the amino groups on the surface of the hydrophilic PEI. The nanoparticles were then dialyzed in PBS using a dialysis membrane (MWCO: 1000 Da) for a further 24 h. This concentration of the GA-PEPE solution was diluted in the medium to match the GA-modified concentration reviewed in the literature above. Figure 1 shows the scheme of the study. It is worthy to note that the previous work showed that 100 μM (0.017g/l) GA has significant anti-inflammatory activity and proper cell viability.[50] By comprehensively considering the concentration ratio of biotargeted molecule-modified nanoparticles and nanoparticle loaded drugs,[24,35] the study finally determined the GA content for modifying PEPE (M_{PEPE}:M_{GA} = 10:1).

In addition, to elucidate the reaction principle of GA and PEPE, a mixture of 5 mg of PEPE and 5 mg of GA was reacted in 5 mL of a DMF−water mixture (V_{DMF}:V_{water} = 1:4) for 24 h. The reaction was then dried under vacuum at 40 °C, and the hydrogen spectrum was detected using AVANCE NEO 400 M HZ NMR in DMSO-d_6. A mixture of 1 g of PEI and 1 g of GA was stirred in water for 24 h at room temperature and then dried under vacuum before comparing the IR spectra of the products and reactants using an INVENIO-R FTIR spectrometer (Bruker, Karlsruhe, Germany).

Characterization of PEI−PPC−PEI Nanoparticles. For the observation of morphology and size distribution, a drop of the sample solution (concentration = 20 μM) was placed onto a 100-mesh copper grid coated with carbon. About 1 min after deposition, the grid was tapped with a filter paper to remove surface water. The samples were air-dried before measurement. Transmission electron microscopy (TEM) was performed on a JEOL JEM 200FS electron microscope (Akishima, Japan) to further analyze the morphology and size of the nanoparticles. The particle size distribution (nanometers) and zeta potential (mV) of the prepared nanoparticles were determined by dynamic light scattering (DLS) using Zeta Sizer Nano Series (Malvern Instruments, UK). The measurements were conducted at 25 °C, and the results were presented based on the data obtained from 90° scattering angles.

Macrophage Cell culture. The RAW 264.7 macrophage cell line (Sigma-Aldrich, St. Louis, Missouri, USA) was cultured in a high glucose Dulbecco's modified Eagle's medium (DMEM) (ServiceBio, Wuhan, China) supplemented with 10% (v/v) fetal bovine serum (FBS) (Tianhang bio, Hangzhou,

https://doi.org/10.1021/acsomega.4c00261
ACS Omega 2024, 9, 14475−14488

China). The cell culture process was conducted in a humidified incubator maintained at 37 °C with 5% CO_2 monitoring.

Cell Viability Analysis. The cells were initially seeded into 96-well plates at a concentration of 1×10^5 cells/mL and incubated in 100 μL of DMEM for 24 h. Following this incubation period, the original medium was replaced with a combined solution of 100 μL DMEM medium and 33 μL of either nanoparticle PBS solution (ranging from 12.5 μM to 200 μM) or GA PBS solution (ranging from 0.025 g/L to 0.4 g/L). The resulting PEPE/GA-PEPE nanoparticles (ranging from 3.125 μM to 50 μM) and the gallic acid solution (ranging from0.00625 g/L to 0.1 g/L) were used as experimental groups in the CCK8 test. The concentration of GA matches the concentration used to synthesize GA-PEPE. The cells were then subjected to another 24 h incubation period. Additionally, a control group was established, in which cells were cultured in 100 μL of DMEM medium with 33 μL of pure PBS, and a blank group was maintained with noncellular pure DMEM medium.

Fluorescence of Live/Dead Staining for Raw264.7. Raw264.7 cells were also seeded in 24-well plates with 1×10^5 cells per well and continuously incubated in 1 mL of DMEM for 24 h. Then, the original medium was replaced with a combined solution of 1 mL DMEM medium and 333 μL of either nanoparticle PBS solution (ranging from 12.5 to 50 μM) or GA PBS solution (ranging from 0.025 to 0.1 g/L). The resulting PEPE/GA-PEPE nanoparticles (ranging from 3.125 to 12.5 μM) and the gallic acid solution (ranging from 0.00625 to 0.025 g/L) were used as experimental groups in the live/dead test. Therefore, cells were washed three times with PBS, and the viability of cells was detected by a calcein-AM/PI double staining kit (Abbkine, Beijing, China) in accordance with manufacture protocols. The results were examined by an inverted fluorescence microscope (Olympus, Tokyo, Japan). The PI-positive cells are red and represented dead cells.

Real-Time Quantitative Polymerase Chain Reaction (PCR) for Antiperiodontitis Evaluation. RAW264.7 cells in DEME were seeded in a 6-well plate at a density of 1×10^6 cells/well and cultured for 24 h in a 5% CO_2 incubator at 37 °C. Subsequently, after the cells reached 80% binding rate, the original media was replaced with fresh FBS-free media containing 1 μg/mL LPS from *Porphyromonas gingivalis* (InvivoGen, France) to establish a periodontitis cell model. This medium was then incubated for another 24 h with 666 μL of nanoparticle solution (from 12.5 to 50 μM) or GA PBS solution (ranging from 0.025 to 0.1 g/L) added at the same culture condition. The concentration settings were consistent with cell death staining. After this, 666 μL of PBS and DMEM medium containing 1ug/mL were added to culture raw264.7 as the inflammatory group. In addition, to establish a control group, DMEM medium without FBS and LPS but with 666 μL of PBS were added.

Following this, the cells were washed twice with PBS and lysed using the TRIZOL reagent (Invitrogen, Thermo Fisher Scientific, Waltham, MA, USA) to isolate the total RNA. The purity and concentration of the RNA were subsequently assessed using a Nanodrop One (Thermo Fisher Scientific, Waltham, MA, USA). For the quantification of mRNA levels, a quantitative reverse transcription PCR (qRT-PCR) technique was employed. Initially, 1 μg of RNA was subjected to cDNA synthesis using UnionScript First-strand cDNA Synthesis Mix for qPCR and dsDNase (Genesand Biotech Co, Beijing, China). This involved incubation at 37 °C for 2 min, followed by reverse transcription at 55 °C for 15 min and enzyme inactivation at 85 °C for 5 min. The UnionScript First-strand cDNA Synthesis Mix used during this process contained UnionScript reverse transcriptase with its buffer, Rnasin, dNTPs, Oligo(dT)20VN, and random primers. Subsequently, real-time qPCR was carried out on 25 ng of cDNA using a QuantStudio 1 Plus Real-Time PCR system (Applied Biosystems, Thermo Fisher Scientific, Waltham, MA, USA) with GS AntiQ qPCR SYBR Green FAST MIX (Genesand Biotech Co, Beijing, China) and 0.5 μM of each of the forward and reverse primers for TNF-α, IL-6, IL-1β, and β-actin obtained from Sangon Biotech Co. (Shanghai, China). The primer sequences used were referenced to published studies and are detailed in Table S2.[51,52]

Statistical Analysis. The data for the anti-inflammatory array characterization were all presented as mean ± SEM. To ensure a normal distribution of the data, a histogram was utilized to visually inspect the data points for each group. Following visual confirmation of the normal distribution, the data were then subjected to analysis. Specifically, CCK8 results were analyzed using two-way ANOVA, while the qPCR results for each gene were analyzed using one-way ANOVA. Subsequently, the Dunnett multiple comparisons test was applied to the results, using GraphPad Prism (v.9, GraphPad Software, San Diego, CA, USA). Any pairwise comparisons exhibiting an adjusted p-value of <0.05 were deemed statistically significant.

RESULTS AND DISCUSSION

Molecular Docking with Gallic Acid. The protein structure of TLR2 (PDB ID: 1FYW) and the TLR4/MD2 complex (PDB ID: 2Z64) was obtained from the PDB database, and the docking pattern with the lowest binding affinity (kcal/mol) was visualized with PyMOL (Table 1). The obtained results showed that TLR2 and GA formed four hydrogen bonds, including SER-784, LYS-783, and ASP-642 (affinity: −3.65 kcal/mol) (Figure 2A). TLR4/MD2 complex and GA also formed four hydrogen bonds, including GLU-593, TRP-590, and LEU-568 (affinity: −3.4 kcal/mol) (Figure 2B). Molecular docking demonstrated the feasibility of targeted binding of GA and TLRs, with the *o*- benzene-triol structure and carbon−oxygen double bond of GA playing an important role.

Table 1. Binding Energy Rank

rank	binding affinity of TLR2[a]	binding affinity of TLR4[a]
1	−3.65	−3.4
2	−2.73	−2.49
3	−3.32	−2.49
4	−3.09	−2.18
5	−2.87	−2.35
6	−2.84	−2.26
7	−2.66	−2.25
8	−2.56	−2.25
9	−2.55	−2.21
10	−2.53	−2.17

[a]Binding affinity of gallic acid and TLR2/TLR4, kcal/mol.

Synthesis of PEI−PPC−PEI. Initially, PPC diols were synthesized through the ring-opening polymerization of CO_2 and PO. Then, the two terminal hydroxyl groups of PPC were modified to carboxyl groups using succinic anhydride. Verification of the successful synthesis of HOOC-PPC−COOH was achieved through acid value determination, as outlined in Table 2. Following this, the amphiphilic block polymers of PEI−PPC−PEI were synthesized via the DCC/

https://doi.org/10.1021/acsomega.4c00261
ACS Omega 2024, 9, 14475−14488

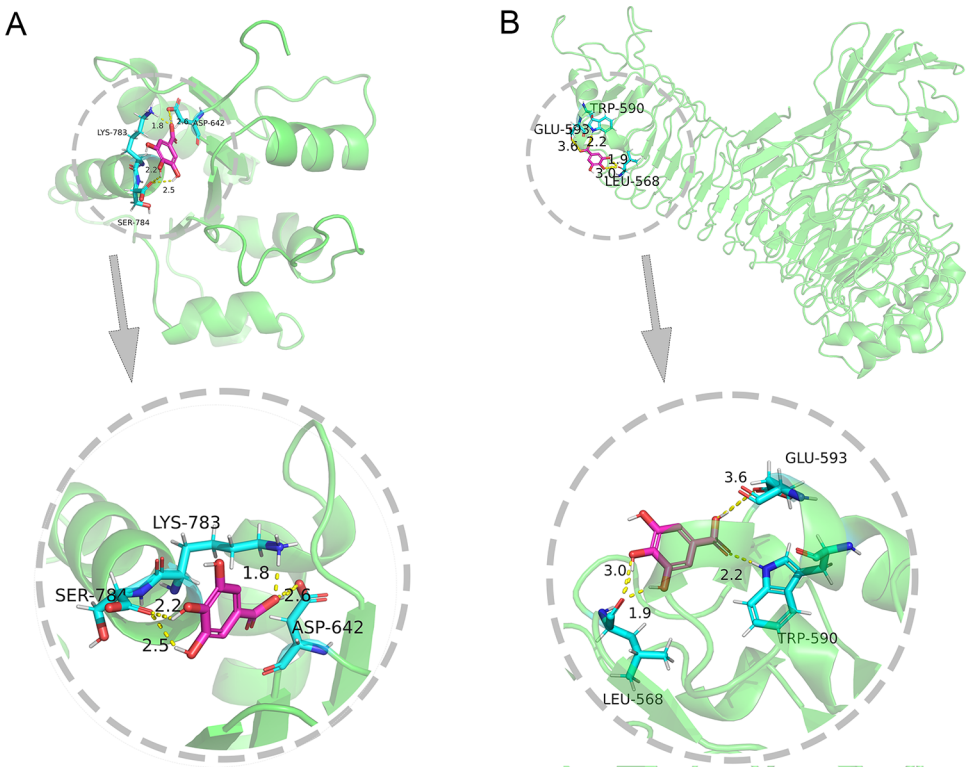

Figure 2. Binding model with the lowest affinity of GA and TLRs. (A) GA binds with TLR2; (B) GA binds with the TLR4/MD2 complex.

Table 2. Acid Value of PPC and HOOH-PPC−COOH

polymers	acid value[a] (mg KOH/g)
PPC	2.6921
HOOC-PPC−COOH	6.5905

[a]Acid values measured by potassium hydroxide ethanol titration.

NHS method in conjunction with branched PEI (Mw:1800) in DMF solvent. The resultant polymers were then purified utilizing a dialysis membrane with an MWCO of 8000−14000. Table 3 shows the molecular weights with PDI of PPC

Table 3. Molecular Weight of PPC and PEI−PPC−PEI

polymer	Mn (kg/mol)[a]	PDI[a]
PPC	15.8	1.28
PEI−PPC−PEI	19.4	1.94

[a]The results were measured by GPC.

and PEI−PPC−PEI polymers measured by the GPC method. The acid value and molecular weight results were in approximate agreement. PEI−PPC−PEI was characterized using ^{1}H NMR of the $CDCl_3$ solvent (Figure 3A). The NMR spectra indicated signals at 4.19 ppm of "peak d" and 5.04 ppm of "peak e", which were attributed to the hydrogen of CH_2 and CH groups, respectively, within the PPC's polycarbonate segments of PEI−PPC−PEI. Additionally, signals at 3.55 ppm of "peak c" and 3.60 ppm of "peak f" were assigned to the hydrogen of CH_2 and CH groups within the PPC's polyether segments of PEI−PPC−PEI. Notably, the characteristic peak at 2.56 ppm of "peak b" corresponding to PEI's amino signal was evident in the NMR spectra of PEI−PPC−PEI. However, it is worth mentioning that the methylene signal (1.97 and 1.27 ppm) of PEI may be masked by a cluster of methyl signaling in "a peak" originating from the PPC (1.32 ppm).[53] Based on the resulting data, it can be concluded that the successful synthesis of the PEI−PPC-PEI amphiphilic block copolymer was achieved.

Synthesis of Gallic Acid-Modified PEI−PPC−PEI Nanoparticles. The formation of the GA-PEPE nanoparticles was evaluated carefully. Figure 3B shows the NMR hydrogen spectra of GA, GA-PEPE, and PEPE in DMSO-d_6. The integration ratios of the signal peaks for the carboxyl group ("h" peak: 12.2 ppm), para-hydroxyl group ("j" peak: 8.81 ppm), interstitial hydroxyl group ("k" peak: 9.16 ppm), and neighboring benzene ring hydrogen ("i" peak: 6.93 ppm) of GA were determined to be 1:1:2:2. Upon inspection of the hydrogen spectrogram of GA-PEPE, the carboxyl signal peak was absent. The three hydroxyl signal peaks exhibited deformation into a broad, flat, dwarf peak ("l" peak: 9.53 ppm), with an integration ratio of approximately 3:2 with the benzene ring hydrogen ("i" peak: 6.93 ppm). The amino signal peak at 2.55 ppm also displayed some alteration. The presence of stretching vibrations of C═O bonds (1650 cm^{-1}), N−H bond bending vibration (1505 cm^{-1}), and C−N bond stretching vibration (1238 cm^{-1}) in FTIR of PEI-GA were observed, which cannot be found in PEI and GA's FTIR (Figure 4).

Frankly speaking, the original intention at the initial stage of the study was to load GA via PEPE nanoparticles for drug delivery of GA. Following the process outlined in the previous literature,[35,54] the drug-loaded nanoparticles exhibited significant discoloration, attributable to the interaction between the amino group on the PEI block and the benzene ring of GA.[55] However, after the dialysis procedure for the fabrication of GA-PEPE nanoparticles, the discoloration persisted. This observation forces us to face the fact that GA reacts with PEPE.

According to the infrared spectroscopy and NMR hydrogen spectrum results, the amino group of PEI amidated with the carboxyl group of GA. The pyrogallol structure of GA is believed

https://doi.org/10.1021/acsomega.4c00261
ACS Omega 2024, 9, 14475−14488

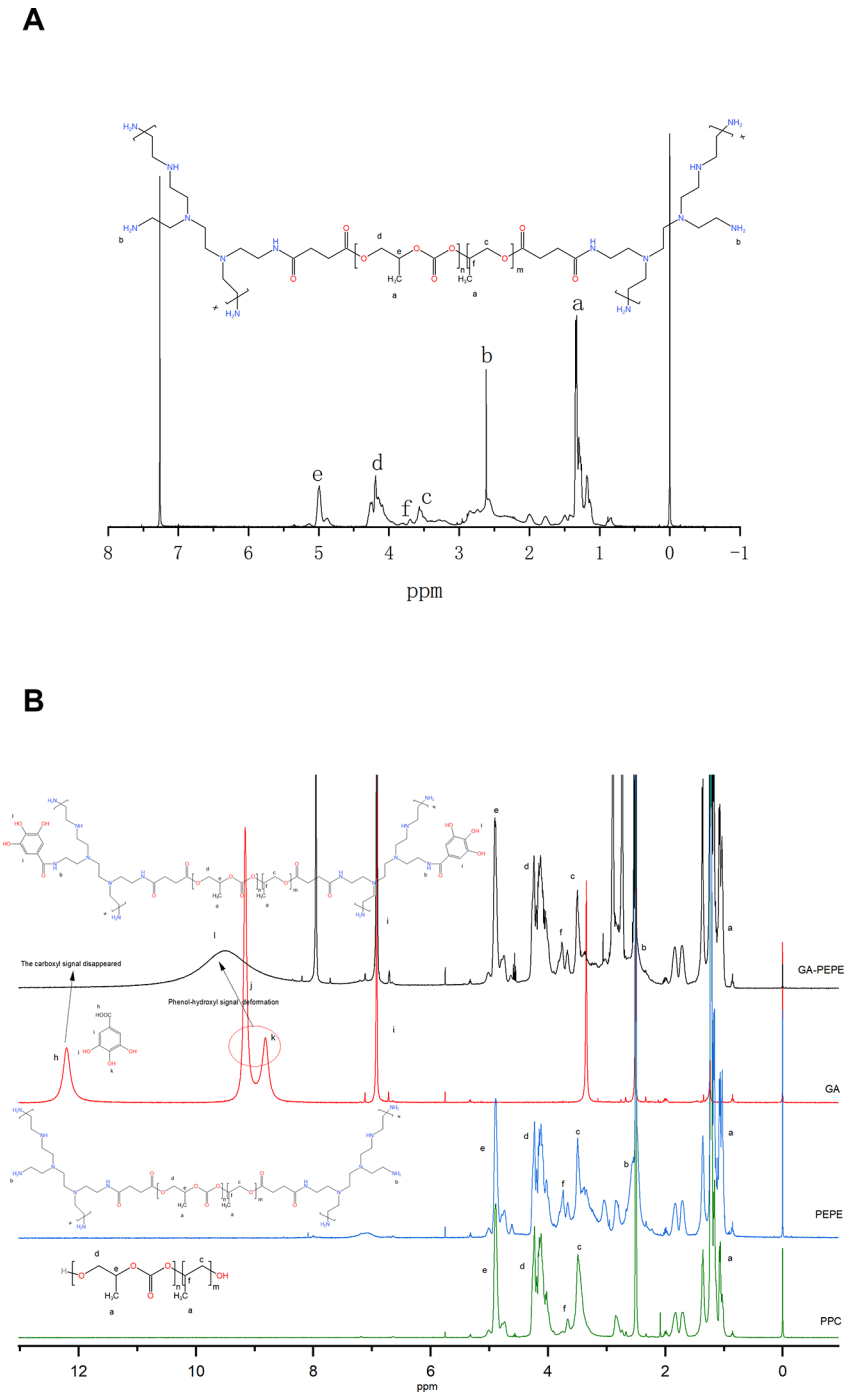

Figure 3. ^{1}H NMR spectra of PEPE and GA-PEPE. (A) ^{1}H NMR spectra of PEPE in $CDCl_3$. The respective characteristic peaks of PEI and PPC can be seen; (B) ^{1}H NMR spectra of PEPE, GA-PEPE, and GA in DMSO-d_6. The disappearance of the carboxyl peaks and the merging of the phenolic hydroxyl peaks were observed. The group of peaks at 7.95, 2.89, and 2.73 ppm are residual DMF stray peaks.

to facilitate the amidation reaction between the carboxyl groups in this system and the PEI amino groups in an aqueous environment.[55,56] This is consistent with the disappearance of the carboxyl peak in NMR and the formation of amide bonds in the FTIR analysis. The distortion and consolidation of the hydroxyl signal peak results from the hydrogen bonding between the hydroxyl group of GA and the amino group of PEPE.[57,58] The reaction to modify the PEI amino group typically requires special reaction conditions, such as under the DCC/NHS system or other catalytic conditions.[24,59] However, GA offers a more convenient path to modify PEPE nanoparticles under catalytic-free conditions compared with conventional modification methods. In general, this study successfully prepared GA-PEPE nanoparticles suitable for antiperiodontitis applications.

Characterization of PEI−PPC−PEI and GA-PEPE Nanoparticles. We prepared a PBS solution of the nanoparticles by dialysis. The solution showed an overall light blue milky or brown color and could stimulate the Tyndall effect (Supplementary Figure). TEM imaging of PEI−PPC−PEI nanoparticles showed segmented copolymer-formed nanoparticles with spherical morphology (Figure 5A). Figure 5B shows the average size distribution of PEPE and GA-PEPE nanoparticles

https://doi.org/10.1021/acsomega.4c00261
ACS Omega 2024, 9, 14475−14488

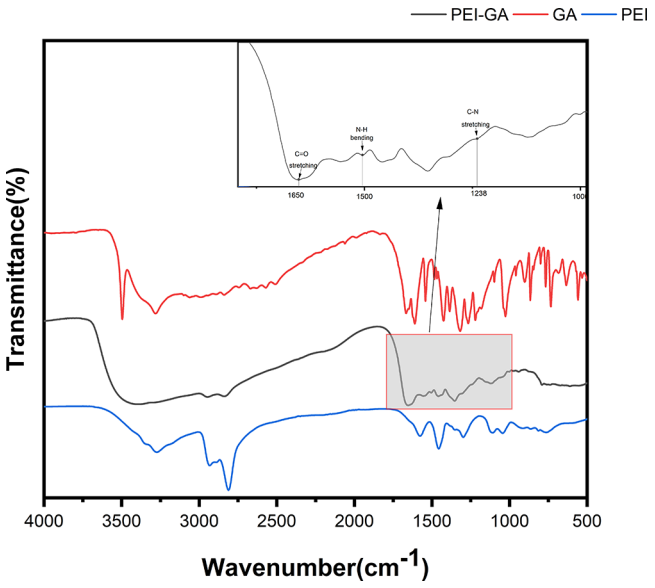

Figure 4. Fourier infrared spectra of PEI-GA, GA and PEI The presence of stretching vibrations of C═O bonds (1650 cm^{-1}), N−H bond bending vibration (1505 cm^{-1}), and C−N bond stretching vibration (1238 cm^{-1}) in FTIR of PEI-GA were observed.

by the intensity three times. The results of the PEPE particles size tests of the DLS are in the following sequence: Z-average 91.19 ± 0.952 nm with 0.129 ± 0.123 PDI. The zeta potential result was +8.99 ± 2.39 mV. While the results of the GA-PEPE particles size tests of the DLS are in the following sequence: Z-average 197 ± 1.229 nm with 0.181 ± 0.006 PDI. The zeta potential result was +6.07 ± 1.02 mV. The PEPE particle sizes of the TEM results and DLS results are relatively close to each other, which indicates that the nanoparticles were not affected by too much hydration during their formation. Nanoparticles of 20−200 nm are usually considered suitable for targeting cells.[60] The positively charged PEPE nanoparticles are due to the highly cationic structure of PEI. Modification of GA resulted in an increase in the particle size of the nanoparticles along with a decrease in the value of the positive charge on the surface. Considering the structure of positively charged nanoparticles, raw264.7 macrophages are more conducive to uptake.[61,62] It is worth emphasizing that different from the traditional electrostatic adsorption binding explanation, the formation of protein corona plays an indispensable role in the high uptake characteristics of positively charged nanoparticles.[63] The modified nanoparticles can also produce more complex uptake characteristics because of the variation of the potential and protein corona.[24,64,65] As the degree of GA grafting introduced by free-radical-induced amidation increases, the particle size of the nanoparticles increases accordingly. Similar results were observed in the present study. Importantly, the antioxidant properties and cytotoxicity also changed proportionally.[66] The physicochemical and biological properties of GA-PEPE under different modification conditions deserve further attention.

Cytocompatibility Results of CCK8 and Live/Dead Staining for Nanoparticles. The results of the CCK8 assay demonstrated that PEPE nanoparticles exhibited cytotoxicity in raw264.7 cells at all concentrations tested (Figure 6A), with significant differences observed in all groups compared to the control group ($p < 0.0001$). The lowest concentration of GA (0.00625 g/L) did not show significant cytotoxicity ($p > 0.05$). For higher four kind of concentrations of GA, this difference became more pronounce ($p < 0.01$ for 0.0125 g/L; $p < 0.0001$ for 0.025 g/L, 0.05g/l, 0.1 g/L). In the case of GA-PEPE, concentrations of 3.125, 6.25, and 12.5 μM showed no significant cytotoxicity compared to the control group ($p > 0.05$). However, as the concentration of GA-PEPE increased to 25 and 50 μM, the cell viability of raw264.7 was significantly reduced ($p < 0.0001$). Around the experimental group at the lowest three concentrations, the results of cell live and death staining were used to compensate for the shortcomings of CCK8 experiment.[67] Figure 6B−D shows the results of the cell staining. Relatively significant cell death was observed in GA-PEPE at 12.5 μM compared to the control group, while the degree of cell death in PEPE at 3.125 μM was lower than that in CCK8. In the GA concentration group matched with GA-PEPE, significant cell death was observed at 0.00625 0.0125, and 0.025 g/L GA, which was consistent with CCK8 results.

Our findings indicated that GA-PEPE significantly mitigated the cytotoxicity of GA and PEPE. The reduction of cytotoxicity of the GA component on GA-PEPE stems from the modifying effect of the carboxyl group. The GA-modified PAMAM nanoparticles exhibit the same toxicity modifying effect.[68] Although biocompatible PPC with superior biocompatibility was used to synthesize PEPE nanoparticles, the cytotoxicity originating from PEI cannot be ignored. The hydrophilic PEI chain segments, the "shells" of the nanoparticles, exhibit cytotoxicity due to the highly positively charged structure of the surface. Such cytotoxicity is manifested in DNA damage.[69] The toxicity of PEI greatly limits the potential of PEI nanoparticles for gene delivery and gene therapy.[70] It is well established that modifying PEI nanoparticles with amines significantly reduces their cytotoxicity.[71−73] The modified PEI nanoparticles have better performance in DNA/RNA delivery and tumor therapy.[74−76] Therefore, low cytotoxicity GA-PEPE is easy to modify and has a broader application prospect in gene targeted therapy and anti-inflammatory strategies.

Anti-Inflammation Characterization of Gallic Acid-Modified PEI−PPC−PEI Nanoparticles by RT-qPCR. After considering the superior cytocompatibility of GA-PEPE below 12.5 μM and the reported anti-inflammatory dose response information of GA,[50,77] the experimental groups with the three lowest concentrations (3.125−12.5 μM PEPE/GA-PEPE and 0.00625−0.025 g/L GA) were set up for anti-inflammatory evaluation. Lipopolysaccharide from *Porphyromonas gingivalis* was successfully used to induce a cellular model of periodontitis. The anti-inflammatory capacity of GA-PEPE was evaluated by measuring the mRNA levels of pro-inflammatory factors IL-6, TNF-α, and IL-1β using RT-qPCR (Figure 7A). The addition of LPS as well as PBS significantly increased the relative levels of pro-inflammatory factors (TNF-α: $p < 0.05$, IL-6 and IL-1β: $p < 0.0001$) compared to the control group. A total of 3.125 μM GA-PEPE performed the characteristic of certain anti-inflammation property with reduction in IL-6 and IL-1β (IL-6: $p < 0.0001$ and IL-1β: $p < 0.05$), although the reduction in TNF-α was not significant (TNF-α: $p > 0.05$). The anti-inflammatory properties of 6.25 μM GA-PEPE were very significant (TNF-α: $p < 0.001$, IL-6: $p < 0.0001$ and IL-1β: $p < 0.001$). However, GA-PEPE at 12.5 μM demonstrated significant anti-inflammatory capacity only in the IL-6's relative level ($p < 0.0001$). Compared to the inflammation model group, 12.5 μM of GA-PEPE instead demonstrated upregulation of TNF-α and IL-1β ($p < 0.0001$) levels. After GA treatment (Figure 7B), the expression of TNF-α and IL-1β decreased significantly compared with the inflammatory group ($p < 0.0001$), but the change of IL-6 was not

https://doi.org/10.1021/acsomega.4c00261
ACS Omega 2024, 9, 14475−14488

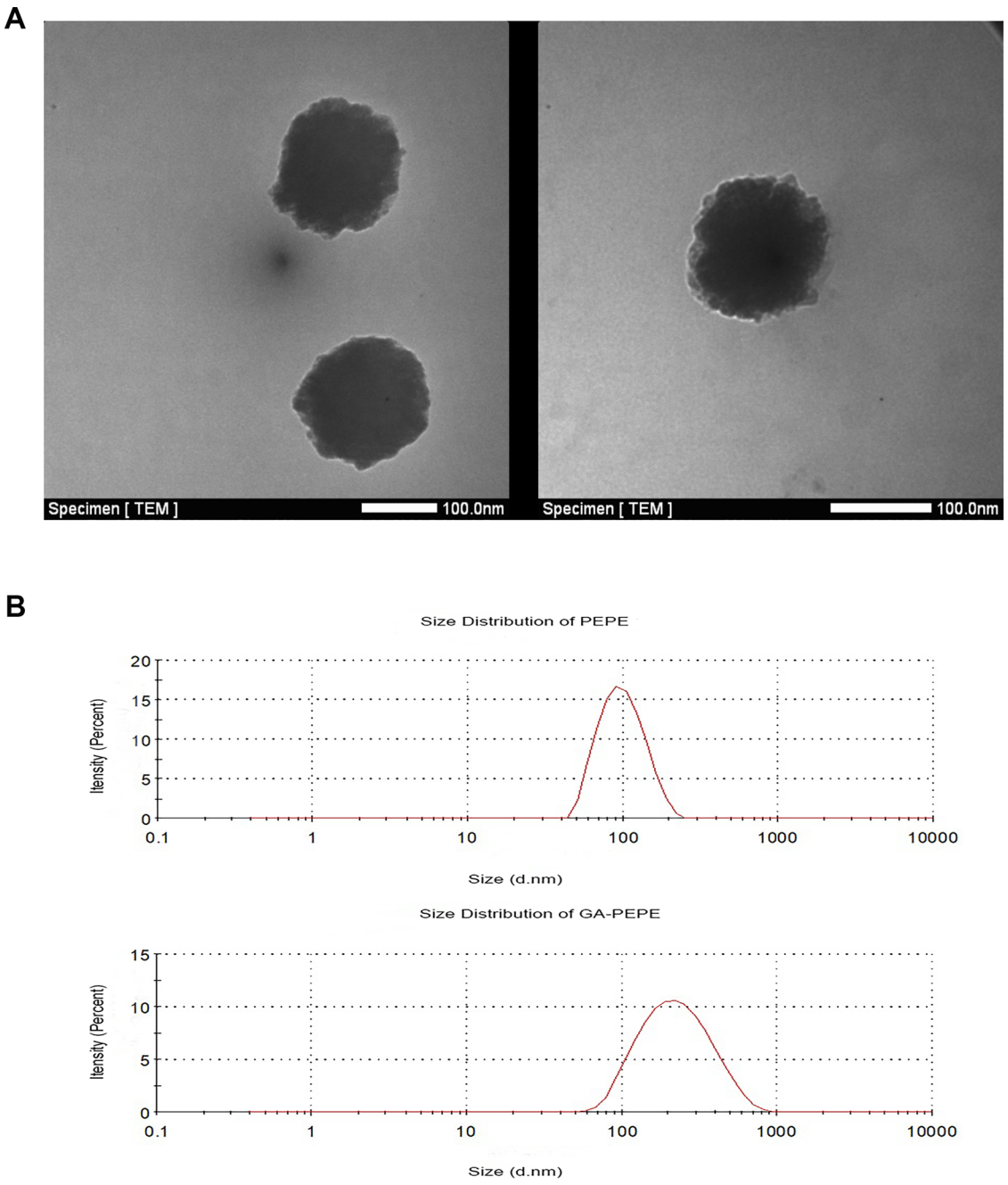

Figure 5. TEM image of PEPE and size distribution of PEPE and GA-PEPE. (A) TEM figure of PEPE. (B) Size distribution of PEPE and GA-PEPE.

significant. Meanwhile, after 0.025 g/L treated, the anti-inflammatory activity of TNF-α and IL-1β decreased and the expression of IL-6 was upregulated. Figure 7C shows that the expression of inflammatory factors after PEPE treatment was significantly increased compared with that in the inflammatory group ($p < 0.01$). Only 3.125 and 6.25 μM PEPE showed no significant changes in IL-1β and TNF-α, respectively ($p > 0.05$), while 3.125 μM PEPE decreased TNF-α levels to a certain extent ($p < 0.01$).

In this study, we successfully induced a macrophage model of inflammation by stimulating TLR2 and TLR4. Unlike conventional LPS, *Porphyromonas gingivalis*' LPS has the unique ability to activate both TLR2 and TLR4, thereby inducing inflammation.[78] The molecular docking simulation has expanded the pool of potential drug aimed at targeting TLRs, showcasing strong binding energy interactions in research within the same field.[79] Alternatively, developing modified nanoparticles to retain the structure of o-triphenol could serve as a novel approach for treating periodontitis by targeting TLRs.[80] Therefore, GA-modified PEPE nanoparticles have been developed to achieve antiperiodontitis strategies targeting TLR. GA-loaded nanoparticles require additional attention to the release characteristic, and the GA-modified PEPE nanoparticles developed in this study are based on the strategy of biocoupled nanoparticles with more efficient drug loading capacity.[81,82]

The anti-inflammatory properties of GA were generally demonstrated in the current study, but the changes in IL-6 showed inconsistent results.[83,84] Additional validation results from translational genomics are necessary. Considering that the anti-inflammatory effects of 3.125 and 6.25 μM GA-PEPE were

https://doi.org/10.1021/acsomega.4c00261
ACS Omega 2024, 9, 14475−14488

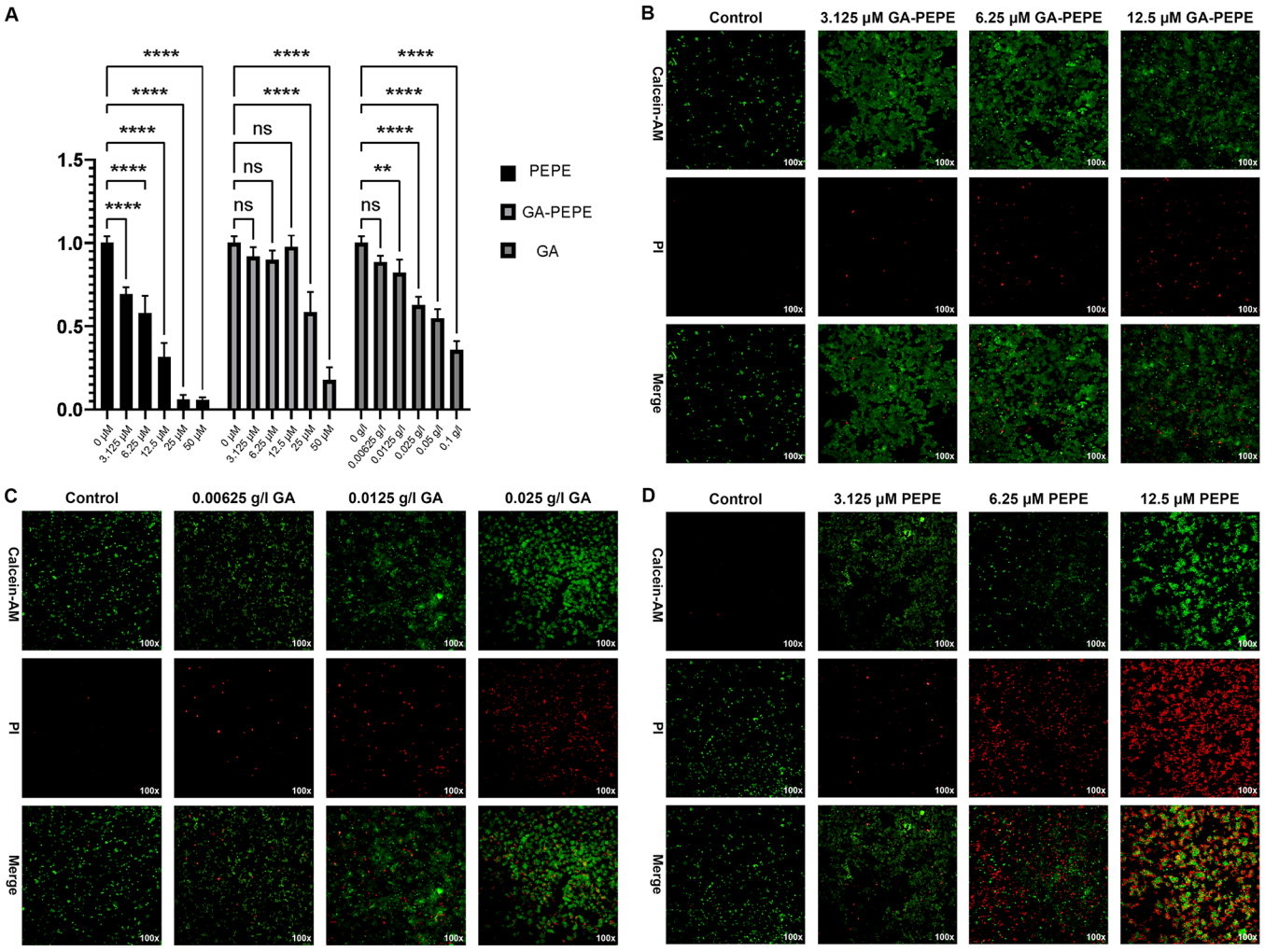

Figure 6. CCK8 and living/death staining results of PEPE, GA-PEPE, and GA for macrophage. (A) CCK8 results of PEPE, GA-PEPE, and GA. Data were referenced to the cell viability of the control group (100%). Data were presented as means ± SD ($n = 3$); (B) live/dead staining results of PEPE; (C) live/dead staining results of GA; (D) live/dead staining results of PEPE. Calcein-AM: calcineurin-AM labels living cells with green fluorescence, PI: pyridinium iodide labels death cells with red fluorescence. The microscope images were taken at 100 times the field of view. PEPE, PEI−PPC−PEI nanoparticles; GA, gallic acid; GA-PEPE, GA-modified PEPE; ns, no significance; *, $p < 0.05$; **, $p < 0.01$; ***, $p < 0.001$; ****, $p < 0.0001$.

also proven, it is necessary to discuss the potential anti-inflammatory mechanism of GA-PEPE. GA has been demonstrated to mitigate the expression of inflammatory cytokines induced by lipopolysaccharides (LPS) in macrophages. This effect is achieved through the inhibition of NLRP3 inflammasome activation and regulation of the NF-κB signaling pathway, both of which are closely linked to toll-like receptors (TLRs). Additionally, GA promotes the upregulation of nuclear factor E2-related factor 2 (Nrf2) and concurrently lowers the production of reactive oxygen species (ROS).[50,77,85−87] In addition, immunofluorescence detection using corresponding antibodies to label macrophages with M1 pro-inflammatory phenotype or M2 anti-inflammatory phenotype is conducive to exploring the inflammatory state.[88] Although a decrease in M1 phenotype and an increase in M2 phenotype have been observed in numerous anti-inflammatory studies involving GA, recent studies suggest that GA may be involved in inhibition of M2 phenotype to alleviate tissue fibrosis.[89−91] The anti-inflammatory effects of GA-PEPE are likely due to its antioxidant polyphenol structure and its targeting of the TLR anti-inflammatory pathway. Further exploration is necessary to understand the changes in the macrophage phenotype in this study and its connection to the inflammatory status.

We observed that the anti-inflammatory effect of GA-PEPE increased with an increasing concentration. The trend was consistent, as the GA concentration increased in the same manner. However, when the concentration reached 12.5 μM, a decrease in the anti-inflammatory effect was noted, accompanied by an upregulation of the expression of TNF-α and IL-1β. This phenomenon suggests a concentration-dependent relationship in the effectiveness of GA, where low concentrations exhibit anti-inflammatory properties, whereas high concentrations display heightened cytotoxicity and may even lead to cell necrosis.[92,93] Combining the results of CCK8 analysis and cell viability staining in the PEPE group revealed a noteworthy escalation in cell death in accordance with concentration levels, aligned with observed alterations in IL-6 and IL-1β.

IL-1β is closely linked to pyroptosis and plays a key role in activating necroptosis, while TNF-α is known as an initiator of necroptosis with a positive feedback influence on the process.[94,95] Caspase-8 deficiency or inhibition can trigger necroptosis.[94] A study blocking Caspase-8 showed significant

https://doi.org/10.1021/acsomega.4c00261
ACS Omega 2024, 9, 14475−14488

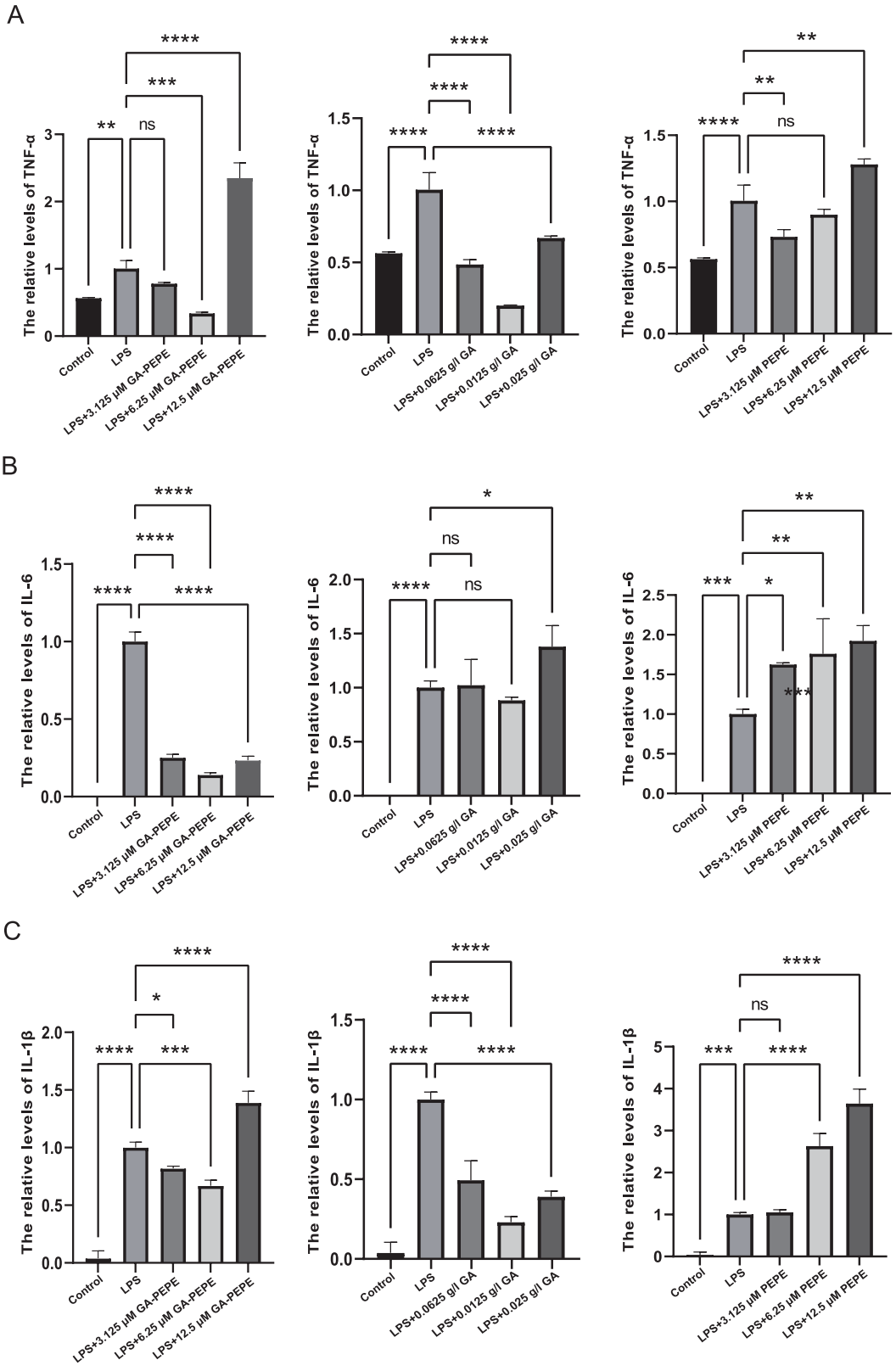

Figure 7. Relative levels of pro-inflammation factors for evaluating anti-inflammation properties of GA-PEPE nanoparticles. (A) Relative levels of TNF-α; (B) relative levels of IL-6; (C) relative levels of IL-1β. Data were referenced to the expression level of the inflammation group (LPS group) and were presented as means ± SD (n = 3). GA, gallic acid; GA-PEPE, GA-modified PEPE; ns, no significance; *, $p < 0.05$; **, $p < 0.01$; ***, $p < 0.001$; ****, $p < 0.0001$.

changes in the expression pattern of IL-1β, while TNF-α and IL-6 changed inconsistently.[96] Another idea that should not be overlooked is that IL-1β- and TNF-triggered macrophage pyroptosis can form pore-induced intracellular traps (PITs), a structure that can be effective in controlling pathogenic infections.[97] This suggests that cell death regulates the

https://doi.org/10.1021/acsomega.4c00261
ACS Omega 2024, 9, 14475−14488

expression of these pro-inflammatory factors, making them not always consistent with the expression trends in the traditional inflammatory paradigm. We combined the results of cell death staining with CCK8 and found that 12.5 μM GA-PEPE actually had a considerable degree of cell death, although the type of death was not clear. The integration of CCK8 data, cell live−dead staining observations, and RT-qPCR findings suggests the plausibility of inferring that the atypical fluctuations in inflammatory factors may be linked to cellular demise.

Elucidating the shortcomings of this process is essential. There is a lack of more direct test evidence that shows that PEPE targets TLRs. Next, it was not in time to elucidate the possible targeting of necroptosis-like pathways activated by high concentrations of PEPE. In vivo studies have more directly assessed the biological distribution and pharmacokinetics of nanoparticles.[98] The size, potential, and modification of targeted molecules all clearly affect the biological distribution of nanoparticles.[98,99] At the same time, the biodegradability of nanoparticles ensures the ability of renal excretion, ensuring the premise of safe pharmacokinetics.[99,100] Because GA-PEPE has special targeted modification and good PPC degradability, it will be very valuable to study its biological distribution and pharmacokinetics.[101]

Overall, GA-PEPE nanoparticles are promising anti-inflammatory nanoparticles. Applying precise targeting strategies and modeling the pharmacokinetics of nanomedicines on periodontitis are opportunities and challenges for GA-PEPE in future work.[98,102] Meanwhile, determining the changes in the molecular conformation of TLR under the influence of PEPE is a priority of future work.

CONCLUSIONS

In this study, the potential binding ability of gallic acid and the TLR2 or TLR4 complex was analyzed by molecular docking. Meanwhile, an amphiphilic block copolymer of PEI−PPC−PEI was synthesized. This amphiphilic block copolymer can self-assemble to form nanoparticles with a particle size of about 91.19 nm. Finally, the PEPE nanoparticles were modified with gallic acid. Cellular experiments showed that gallic acid modification could significantly improve the biocompatibility of PEPE nanoparticles. Also, 6.25 μM of GA-PEPE significantly reduced the relative levels of inflammatory macrophage pro-inflammatory factors TNF-α, IL6, and IL-1β. GA-PEPE has shown very promising antiperiotitis potential; however, the exact mechanism of how GA-PEPE affects TLRs is unclear, which will be explored in depth in subsequent studies.

ASSOCIATED CONTENT

Data Availability Statement

All data generated or analyzed during this study are included in this published article [and its Supporting Information files].

Supporting Information

The Supporting Information is available free of charge at https://pubs.acs.org/doi/10.1021/acsomega.4c00261.

(Table S1) Instrument parameters of hydrogen magnetic resonance spectroscopy, (Table S2) primers used in this study, and supplementary pictures of the PEPE and GA-PEPE Tyndall effect. (PDF)

AUTHOR INFORMATION

Corresponding Authors

Yuyan Liu − *Department of endodontics, Jilin University, Hospital of stomatology, Changchun 130041, China*; Email: liuyyli@163.com

Fengxiang Gao − *Chinese Academy of Sciences, Changchun Institute of Applied Chemistry, Changchun 130022, China*; Email: gfx26@ciac.ac.cn

Authors

Zunxuan Xie − *Department of endodontics, Jilin University, Hospital of stomatology, Changchun 130041, China*; orcid.org/0000-0002-8994-3229

Boyang Gao − *Department of endodontics, Jilin University, Hospital of stomatology, Changchun 130041, China*

Jinyao Liu − *Department of endodontics, Jilin University, Hospital of stomatology, Changchun 130041, China*

Jiaming He − *Department of endodontics, Jilin University, Hospital of stomatology, Changchun 130041, China*

Complete contact information is available at: https://pubs.acs.org/10.1021/acsomega.4c00261

Author Contributions

Conceptualization was done by Z.X., B.G., Y.L., and F.G.; methodology was developed by Z.X., B.G., Y.L., and F.G.; software was developed by Z.X.; validation was performed by Z.X., B.G., and J.L.; formal analysis was done by Z.X.; investigation was performed by Z.X., J.L., and J.H.; resources were gathered by Z.X., Y.L., and F.G.; data curation was done by Z.X. and B.G.; writing—original draft preparation—was done by Z.X.; writing—review and editing was done by Z.X., Y.L., and F.G.; visualization was performed by Z.X.; supervision was done by F.G.; project administration was done by Z.X., Y.L., and F.G.; funding acquisition was performed by Y.L. All authors have read and agreed to the published version of the manuscript.

Funding

This research and APC was funded by Technology and science project of Department of finance, Jilin Province, grant number JCSE2021893−26.

Notes

The authors declare no competing financial interest.

ACKNOWLEDGMENTS

Acknowledgement of the technical testing provided by the Changchun Institute of Applied Chemistry.

REFERENCES

(1) Kwon, T.; Lamster, I. B.; Levin, L. Current Concepts in the Management of Periodontitis. *Int. Dent J.* **2021**, *71* (6), 462−76.

(2) Slots, J. Periodontitis: facts, fallacies and the future. *Periodontol 2000.* **2017**, *75* (1), 7−23.

(3) Kawai, T.; Akira, S. The role of pattern-recognition receptors in innate immunity: update on Toll-like receptors. *Nat. Immunol.* **2010**, *11* (5), 373−84.

(4) Heinbockel, L.; Weindl, G.; Martinez-de-Tejada, G.; Correa, W.; Sanchez-Gomez, S.; Bárcena-Varela, S.; et al. Inhibition of Lipopolysaccharide- and Lipoprotein-Induced Inflammation by Antitoxin Peptide Pep19−2.5. *Front. Immunol.* **2018**, *9*, 1704.

(5) Jurdziński, K. T.; Potempa, J.; Grabiec, A. M. Epigenetic regulation of inflammation in periodontitis: cellular mechanisms and therapeutic potential. *Clin. Epigenet.* **2020**, *12* (1), 186.

(6) Ozturk, A.; Vieira, A. R. TLR4 as a risk factor for periodontal disease: a reappraisal. *J. Clin Periodontol.* **2009**, *36* (4), 279−86.

(7) Marcano, R.; Rojo, M. Á.; Cordoba-Diaz, D.; Garrosa, M. Pathological and Therapeutic Approach to Endotoxin-logical and Therapeutic Approach to EndotoxiSecreting Bacteria Involved in Periodontal Disease. *Toxins* **2021**, *13* (8), 533 DOI: 10.3390/toxins13080533.
(8) Ryu, J. K.; Kim, S. J.; Rah, S. H.; Kang, J. I.; Jung, H. E.; Lee, D.; et al. Reconstruction of LPS Transfer Cascade Reveals Structural Determinants within LBP, CD14, and TLR4-MD2 for Efficient LPS Recognition and Transfer. *Immunity.* **2017**, *46* (1), 38−50.
(9) Simpson, M. E.; Petri, W. A., Jr. TLR2 as a Therapeutic Target in Bacterial Infection. *Trends Mol. Med.* **2020**, *26* (8), 715−7.
(10) Karimy, J. K.; Reeves, B. C.; Kahle, K. T. Targeting TLR4-dependent inflammation in post-hemorrhagic brain injury. *Expert Opin Ther Targets.* **2020**, *24* (6), 525−33.
(11) Boarescu, I.; Pop, R. M.; Boarescu, P. M.; Bocşan, I. C.; Gheban, D.; Râjnoveanu, R. M.; et al. Anti-Inflammatory and Analgesic Effects of Curcumin Nanoparticles Associated with Diclofenac Sodium in Experimental Acute Inflammation. *Int. J. Mol. Sci.* **2022**, *23* (19), 11737 DOI: 10.3390/ijms231911737.
(12) Yan, F.; Zhong, Z.; Wang, Y.; Feng, Y.; Mei, Z.; Li, H.; et al. Exosome-based biomimetic nanoparticles targeted to inflamed joints for enhanced treatment of rheumatoid arthritis. *J. Nanobiotechnol.* **2020**, *18* (1), 115.
(13) Ni, C.; Zhou, J.; Kong, N.; Bian, T.; Zhang, Y.; Huang, X.; et al. Gold nanoparticles modulate the crosstalk between macrophages and periodontal ligament cells for periodontitis treatment. *Biomaterials.* **2019**, *206*, 115−32.
(14) Neu, M.; Fischer, D.; Kissel, T. Recent advances in rational gene transfer vector design based on poly(ethylene imine) and its derivatives. *J. Gene Med.* **2005**, *7* (8), 992−1009.
(15) Shi, S.; Guo, Q.; Kan, B.; Fu, S.; Wang, X.; Gong, C.; et al. A novel Poly(ε-caprolactone)-Pluronic-Poly(ε-caprolactone) grafted Polyethyleneimine(PCFC-g-PEI), Part 1, synthesis, cytotoxicity, and in vitro transfection study. *BMC Biotechnol.* **2009**, *9*, 65.
(16) Ratanajanchai, M.; Lee, D. H.; Sunintaboon, P.; Yang, S. G. Photo-cured PMMA/PEI core/shell nanoparticles surface-modified with Gd-DTPA for T1MR imaging. *J. Colloid Interface Sci.* **2014**, *415*, 70−6.
(17) Wu, Y.; Zhang, Y.; Zhang, W.; Sun, C.; Wu, J.; Tang, J. Reversing of multidrug resistance breast cancer by co-delivery of P-gp siRNA and doxorubicin via folic acid-modified core-shell nanomicelles. *Colloids Surf. B Biointerfaces.* **2016**, *138*, 60−9.
(18) Xie, X.; Chen, Y.; Chen, Z.; Feng, Y.; Wang, J.; Li, T.; et al. Polymeric Hybrid Nanomicelles for Cancer Theranostics: An Efficient and Precise Anticancer Strategy for the Codelivery of Doxorubicin/miR-34a and Magnetic Resonance Imaging. *ACS Appl. Mater. Interfaces.* **2019**, *11* (47), 43865−78.
(19) Kiani, M. H.; Ali, S.; Qadry, A.; Arshad, R.; Aslam, A.; Shahnaz, G. Polyethylene imine conjugated supramolecular stereocomplexed nanomicelles for intracellular delivery of rifampicin against Mycobacterium bovis. *Colloids Surf. B Biointerfaces.* **2021**, *206*, No. 111976.
(20) Wang, B.; Dong, Y.; Cen, Y.; Chen, S.; Wen, X.; Liu, K.; et al. PEI-PLGA nanoparticles significantly enhanced the immunogenicity of IsdB(137−361) proteins from Staphylococcus aureus. *Immun. Inflammation Dis.* **2023**, *11* (7), No. e928.
(21) Hu, H.; Zhang, Y.; Ji, W.; Mei, H.; Wu, T.; He, Z.; et al. Hyaluronic acid-coated and Olaparib-loaded PEI - PLGA nanoparticles for the targeted therapy of triple negative breast cancer. *J. Microencapsul.* **2022**, *39* (1), 25−36.
(22) Mohammad Gholinia Sarpoli, L.; Zare-Karizi, S.; Heidari, E.; Hasanzadeh, A.; Bayandori, M.; Azedi, F.; et al. Co-delivery of curcumin and Bcl-2 siRNA to enhance therapeutic effect against breast cancer cells using PEI-functionalized PLGA nanoparticles. *Pharm. Dev Technol.* **2022**, *27* (7), 785−93.
(23) Wang, S.; Zhang, J.; Wang, Y.; Chen, M. Hyaluronic acid-coated PEI-PLGA nanoparticles mediated co-delivery of doxorubicin and miR-542−3p for triple negative breast cancer therapy. *Nanomedicine.* **2016**, *12* (2), 411−20.
(24) Sun, X.; Wang, N.; Yang, L. Y.; Ouyang, X. K.; Huang, F. Folic Acid and PEI Modified Mesoporous Silica for Targeted Delivery of Curcumin. *Pharmaceutics* **2019**, *11* (9), 430 DOI: 10.3390/pharmaceutics11090430.
(25) Godbey, W. T.; Wu, K. K.; Mikos, A. G. Poly(ethylenimine) and its role in gene delivery. *J. Controlled Release* **1999**, *60* (2−3), 149−60.
(26) Godbey, W. T.; Wu, K. K.; Mikos, A. G. Poly(ethylenimine)-mediated gene delivery affects endothelial cell function and viability. *Biomaterials.* **2001**, *22* (5), 471−80.
(27) Wu, X. R.; Zhang, J.; Zhang, J. H.; Xiao, Y. P.; He, X.; Liu, Y. H.; et al. Amino Acid-Linked Low Molecular Weight Polyethylenimine for Improved Gene Delivery and Biocompatibility. *Molecules* **2020**, *25* (4), 975 DOI: 10.3390/molecules25040975.
(28) Zhuo, C. W.; Qin, Y. S.; Wang, X. H.; Wang, F. S. Steric hindrance ligand strategy to aluminum porphyrin catalyst for completely alternative copolymerization of CO2 and propylene oxide. *Chin. J. Polym. Sci.* **2018**, *36* (2), 252−260.
(29) Gao, F.-X.; Cai, Y.; Liu, S.-J.; Wang, X.-H. High-Performance Biodegradable PBAT/PPC Composite Film Through Reactive Compatibilizer. *Chinese Journal of Polymer Science.* **2023**, *41* (7), 1051−8.
(30) Weems, A. C.; Arno, M. C.; Yu, W.; Huckstepp, R. T. R.; Dove, A. P. 4D polycarbonates via stereolithography as scaffolds for soft tissue repair. *Nat. Commun.* **2021**, *12* (1), 3771.
(31) Liu, X.; Jiang, Z.; Xing, D.; Yang, Y.; Li, Z.; Sun, Z. Recent progress in nanocomposites of carbon dioxide fixation derived reproducible biomedical polymers. *Front. Chem.* **2022**, *10*, 1035825.
(32) Quan, Z.; Luo, C.; Zhu, B.; Zhao, C.; Yang, M.; Bjørås, M.; et al. Synthesis and antimicrobial activities of chitosan/polypropylene carbonate-based nanoparticles. *RSC Adv.* **2021**, *11* (17), 10121−10129.
(33) Chen, X.; Zhao, S.; Chu, S.; Liu, S.; Yu, M.; Li, J.; et al. A novel sustained release fluoride strip based Poly(propylene carbonate) for preventing caries. *Eur. J. Pharm. Sci.* **2022**, *171*, No. 106128.
(34) Zhong, X.; Lu, Z.; Valtchev, P.; Wei, H.; Zreiqat, H.; Dehghani, F. Surface modification of poly(propylene carbonate) by aminolysis and layer-by-layer assembly for enhanced cytocompatibility. *Colloids and Surfaces B: Biointerfaces.* **2012**, *93*, 75−84.
(35) Li, H.; Niu, Y. Synthesis and characterization of amphiphilic block polymer poly(ethylene glycol)-poly(propylene carbonate)-poly-(ethylene glycol) for drug delivery. *Mater. Sci. Eng. C Mater. Biol. Appl.* **2018**, *89*, 160−5.
(36) Xu, Y.; Tang, G.; Zhang, C.; Wang, N.; Feng, Y. Gallic Acid and Diabetes Mellitus: Its Association with Oxidative Stress. *Molecules* **2021**, *26* (23), 7115 DOI: 10.3390/molecules26237115.
(37) Alves, M. M. M.; Brito, L. M.; Souza, A. C.; Queiroz, B.; de Carvalho, T. P.; Batista, J. F.; et al. Gallic and ellagic acids: two natural immunomodulator compounds solve infection of macrophages by Leishmania major. *Naunyn Schmiedebergs Arch Pharmacol.* **2017**, *390* (9), 893−903.
(38) Park, W. H. Gallic acid induces HeLa cell death via increasing GSH depletion rather than ROS levels. *Oncol. Rep.* **2017**, *37* (2), 1277−83.
(39) Patil, P.; Killedar, S. Chitosan and glyceryl monooleate nanostructures containing gallic acid isolated from amla fruit: targeted delivery system. *Heliyon.* **2021**, *7* (3), No. e06526.
(40) Aldawsari, M. F.; Alkholifi, F. K.; Foudah, A. I.; Alqarni, M. H.; Alam, A.; Salkini, M. A.; et al. Gallic-Acid-Loaded PLGA Nanoparticles: A Promising Transdermal Drug Delivery System with Antioxidant and Antimicrobial Agents. *Pharmaceuticals* **2023**, *16* (8), 1090 DOI: 10.3390/ph16081090.
(41) Hassani, A.; Azarian, M. M. S.; Ibrahim, W. N.; Hussain, S. A. Preparation, characterization and therapeutic properties of gum arabic-stabilized gallic acid nanoparticles. *Sci. Rep.* **2020**, *10* (1), 17808.
(42) Kumar, S.; Sinha, K.; Sharma, R.; Purohit, R.; Padwad, Y. Phloretin and phloridzin improve insulin sensitivity and enhance glucose uptake by subverting PPARγ/Cdk5 interaction in differentiated adipocytes. *Exp. Cell Res.* **2019**, *383* (1), 111480.

(43) Rajasekaran, R.; George Priya Doss, C.; Sudandiradoss, C.; Ramanathan, K.; Purohit, R.; Sethumadhavan, R. Effect of deleterious nsSNP on the HER2 receptor based on stability and binding affinity with herceptin: A computational approach. *Comptes Rendus Biologies.* **2008**, *331* (6), 409−17.
(44) Singh, R.; Bhardwaj, V.; Purohit, R. Identification of a novel binding mechanism of Quinoline based molecules with lactate dehydrogenase of Plasmodium falciparum. *J. Biomol Struct Dyn.* **2021**, *39* (1), 348−56.
(45) Bhardwaj, V. K.; Purohit, R. A new insight into protein-protein interactions and the effect of conformational alterations in PCNA. *International Journal of Biological Macromolecules.* **2020**, *148*, 999−1009.
(46) Bhardwaj, V.; Purohit, R. Computational investigation on effect of mutations in PCNA resulting in structural perturbations and inhibition of mismatch repair pathway. *J. Biomol Struct Dyn.* **2020**, *38* (7), 1963−74.
(47) Kamaraj, B.; Purohit, R. Mutational Analysis on Membrane Associated Transporter Protein (MATP) and Their Structural Consequences in Oculocutaeous Albinism Type 4 (OCA4)-A Molecular Dynamics Approach. *J. Cell Biochem.* **2016**, *117* (11), 2608−19.
(48) Dong, Y.; Wang, X.; Zhao, X.; Wang, F. Facile synthesis of poly(ether carbonate)s via copolymerization of CO 2 and propylene oxide under combinatorial catalyst of rare earth ternary complex and double metal cyanide complex. *J. Polym. Sci. Part A: Polym. Chem.* **2012**, *50* (2), 362−370.
(49) Nam, Y. S.; Kang, H. S.; Park, J. Y.; Park, T. G.; Han, S. H.; Chang, I. S. New micelle-like polymer aggregates made from PEI-PLGA diblock copolymers: micellar characteristics and cellular uptake. *Biomaterials.* **2003**, *24* (12), 2053−9.
(50) Li, K.; Gong, Q.; Lu, B.; Huang, K.; Tong, Y.; Mutsvene, T. E.; et al. Anti-inflammatory and antioxidative effects of gallic acid on experimental dry eye: in vitro and in vivo studies. *Eye Vision* **2023**, *10* (1), 17.
(51) Sun, Y.; Liang, L.; Yi, Y.; Meng, Y.; Peng, K.; Jiang, X.; et al. Synthesis, characterization and anti-inflammatory activity of selenium nanoparticles stabilized by aminated yeast glucan. *International Journal of Biological Macromolecules.* **2023**, *245*, No. 125187.
(52) Alnuqaydan, A. M.; Almutary, A. G.; Azam, M.; Manandhar, B.; De Rubis, G.; Madheswaran, T.; et al. Phytantriol-Based Berberine-Loaded Liquid Crystalline Nanoparticles Attenuate Inflammation and Oxidative Stress in Lipopolysaccharide-Induced RAW264.7 Macrophages. *Nanomaterials* **2022**, *12* (23), 4312 DOI: 10.3390/nano12234312.
(53) Li, Q.; Wang, X. D.; Li, Q. Y.; Yang, J. J.; Zhang, Z. J. New Amphiphilic Polymer with Emulsifying Capability for Extra Heavy Crude Oil. *INDUSTRIAL & ENGINEERING CHEMISTRY RESEARCH.* **2018**, *57* (49), 17013−23.
(54) Chen, J.; Xu, W.; Dai, T.; Jiao, S.; Xue, X.; Jiang, J.; et al. Pioglitazone-Loaded Cartilage-Targeted Nanomicelles (Pio@C-HA-DOs) for Osteoarthritis Treatment. *Int. J. Nanomedicine.* **2023**, *18*, 5871−90.
(55) Zhao, Y.; Zhou, S.; Xia, X.; Tan, M.; Lv, Y.; Cheng, Y.; et al. High-performance carboxymethyl cellulose-based hydrogel film for food packaging and preservation system. *Int. J. Biol. Macromol.* **2022**, *223* (Pt A), 1126−1137.
(56) Zhou, Z.; Roelfes, G. Synergistic Catalysis of Tandem Michael Addition/Enantioselective Protonation Reactions by an Artificial Enzyme. *Acs Catalysis.* **2021**, *11* (15), 9366−9.
(57) Jin, Z. M.; Xu, D. J.; Pan, Y. J.; Xu, Y. Z.; Chiang, M. Y. N. 2:1 complex of 4-methylphenol with piperazine, structure in the solid and solution state. *J. Mol. Struct.* **2001**, *559* (1−3), 1−5.
(58) Nuñez-Dallos, N.; Reyes, A.; Quevedo, R. Hydrogen bond assisted synthesis of azacyclophanes from L-tyrosine derivatives. *Tetrahedron Lett.* **2012**, *53* (5), 530−4.
(59) Noske, S.; Karimov, M.; Aigner, A.; Ewe, A. Tyrosine-Modification of Polypropylenimine (PPI) and Polyethylenimine (PEI) Strongly Improves Efficacy of siRNA-Mediated Gene Knockdown. *Nanomaterials* **2020**, *10* (9), 1809 DOI: 10.3390/nano10091809.
(60) Davis, M. E.; Chen, Z. G.; Shin, D. M. Nanoparticle therapeutics: an emerging treatment modality for cancer. *Nat. Rev. Drug Discovery* **2008**, *7* (9), 771−82.
(61) Shi, Y.; Xu, X.; Yu, H.; Lin, Z.; Zuo, H.; Wu, Y. Defined positive charge patterns created on DNA nanostructures determine cellular uptake efficiency. *Nano Lett.* **2022**, *22* (13), 5330−8.
(62) Liu, X.; Huang, N.; Li, H.; Jin, Q.; Ji, J. Surface and size effects on cell interaction of gold nanoparticles with both phagocytic and nonphagocytic cells. *Langmuir.* **2013**, *29* (29), 9138−48.
(63) Forest, V.; Pourchez, J. Preferential binding of positive nanoparticles on cell membranes is due to electrostatic interactions: A too simplistic explanation that does not take into account the nanoparticle protein corona. *Mater. Sci. Eng.: C* **2017**, *70* (Pt 1), 889−896.
(64) Oberländer, J.; Champanhac, C.; da Costa Marques, R.; Landfester, K.; Mailänder, V. Temperature, concentration, and surface modification influence the cellular uptake and the protein corona of polystyrene nanoparticles. *Acta Biomater.* **2022**, *148*, 271−278.
(65) Liu, C.; Xie, Y.; Li, X.; Yao, X.; Wang, X.; Wang, M.; et al. Folic Acid/Peptides Modified PLGA-PEI-PEG Polymeric Vectors as Efficient Gene Delivery Vehicles: Synthesis, Characterization and Their Biological Performance. *Mol. Biotechnol.* **2021**, *63* (1), 63−79.
(66) Mohamady Hussein, M. A.; Olmos, J. M.; Pierański, M. K.; Grinholc, M.; Buhl, E. M.; Gunduz, O.; et al. Post grafted gallic acid to chitosan-Ag hybrid nanoparticles via free radical-induced grafting reactions. *International Journal of Biological Macromolecules.* **2023**, *233*, No. 123395.
(67) Hou, Y., Zhang, X., Li, J., Wang, L., Guan, S. A multi-functional MgF2/polydopamine/hyaluronan-astaxanthin coating on the biodegradable ZE21B alloy with better corrosion resistance and biocompatibility for cardiovascular application. *J. Magnesium Alloys* **2022**. DOI: 10.1016/j.jma.2022.06.008
(68) Priyadarshi, K.; Shirsath, K.; Waghela, N. B.; Sharma, A.; Kumar, A.; Pathak, C. Surface modified PAMAM dendrimers with gallic acid inhibit, cell proliferation, cell migration and inflammatory response to augment apoptotic cell death in human colon carcinoma cells. *J. Biomol Struct Dyn.* **2021**, *39* (18), 6853−69.
(69) Kim, H. J.; Cho, H. B.; Lee, S.; Lyu, J.; Kim, H. R.; Lee, S.; et al. Strategies for accelerating osteogenesis through nanoparticle-based DNA/mitochondrial damage repair. *Theranostics.* **2022**, *12* (14), 6409−21.
(70) Huang, X.; Shen, S.; Zhang, Z.; Zhuang, J. Cross-linked polyethylenimine-tripolyphosphate nanoparticles for gene delivery. *Int. J. Nanomedicine.* **2014**, *9*, 4785−94.
(71) Cho, K. S.; Kim, S.; Chun, H. B.; Cheon, J. H.; Cho, M. H.; Lee, A. Y.; et al. Efficient gene transfection to lung cancer cells via Folate-PEI-Sorbitol gene transporter. *PLoS One.* **2022**, *17* (5), No. e0266181.
(72) Li, Z.; Liu, Y.; Huang, X.; Hu, C.; Wang, H.; Yuan, L.; et al. One-step preparation of gold nanovectors using folate modified polyethylenimine and their use in target-specific gene transfection. *Colloids Surf. B Biointerfaces.* **2019**, *177*, 306−12.
(73) Luu, Q. P.; Shin, J. Y.; Kim, Y. K.; Islam, M. A.; Kang, S. K.; Cho, M. H.; et al. High gene transfer by the osmotic polysorbitol-mediated transporter through the selective caveolae endocytic pathway. *Mol. Pharmaceutics* **2012**, *9* (8), 2206−18.
(74) Yu, Q.; Zhang, M.; Chen, Y.; Chen, X.; Shi, S.; Sun, K.; et al. Self-Assembled Nanoparticles Prepared from Low-Molecular-Weight PEI and Low-Generation PAMAM for EGFRvIII-Chimeric Antigen Receptor Gene Loading and T-Cell Transient Modification. *Int. J. Nanomedicine.* **2020**, *15*, 483−95.
(75) Kolte, A.; Patil, S.; Lesimple, P.; Hanrahan, J. W.; Misra, A. PEGylated composite nanoparticles of PLGA and polyethylenimine for safe and efficient delivery of pDNA to lungs. *Int. J. Pharm.* **2017**, *524* (1−2), 382−96.
(76) Ewe, A.; Höbel, S.; Heine, C.; Merz, L.; Kallendrusch, S.; Bechmann, I.; et al. Optimized polyethylenimine (PEI)-based nano-

particles for siRNA delivery, analyzed in vitro and in an ex vivo tumor tissue slice culture model. *Drug Deliv Transl Res.* **2017**, *7* (2), 206−16.
(77) Yu, T. Y.; Feng, Y. M.; Kong, W. S.; Li, S. N.; Sun, X. J.; Zhou, G.; et al. Gallic acid ameliorates dextran sulfate sodium-induced ulcerative colitis in mice via inhibiting NLRP3 inflammasome. *Front. Pharmacol.* **2023**, *14*, 1095721.
(78) Reife, R. A.; Coats, S. R.; Al-Qutub, M.; Dixon, D. M.; Braham, P. A.; Billharz, R. J.; et al. Porphyromonas gingivalis lipopolysaccharide lipid A heterogeneity: differential activities of tetra- and penta-acylated lipid A structures on E-selectin expression and TLR4 recognition. *Cell Microbiol.* **2006**, *8* (5), 857−68.
(79) Niu, X.; Yu, Y.; Guo, H.; Yang, Y.; Wang, G.; Sun, L.; et al. Molecular modeling reveals the inhibition mechanism and binding mode of ursolic acid to TLR4-MD2. *Computational and Theoretical Chemistry.* **2018**, *1123*, 73−8.
(80) Song, B.; Zhang, Y. L.; Chen, L. J.; Zhou, T.; Huang, W. K.; Zhou, X.; et al. The role of Toll-like receptors in periodontitis. *Oral Dis.* **2017**, *23* (2), 168−80.
(81) Nemčeková, K.; Svitková, V.; Sochr, J.; Gemeiner, P.; Labuda, J. Gallic acid-coated silver nanoparticles as perspective drug nanocarriers: bioanalytical study. *Anal Bioanal Chem.* **2022**, *414* (18), 5493−505.
(82) Mahboob, T.; Nawaz, M.; de Lourdes Pereira, M.; Tian-Chye, T.; Samudi, C.; Sekaran, S. D.; et al. PLGA nanoparticles loaded with Gallic acid- a constituent of Leea indica against Acanthamoeba triangularis. *Sci. Rep.* **2020**, *10* (1), 8954.
(83) Wang, F.; Stappenbeck, F.; Tang, L. Y.; Zhang, Y. E.; Hui, S. T.; Lusis, A. J.; et al. Oxy210, a Semi-Synthetic Oxysterol, Exerts Anti-Inflammatory Effects in Macrophages via Inhibition of Toll-like Receptor (TLR) 4 and TLR2 Signaling and Modulation of Macrophage Polarization. *Int. J. Mol. Sci.* **2022**, *23* (10), 5478 DOI: 10.3390/ijms23105478.
(84) Zhang, D.; Li, H.; Li, T.; Zhou, M.; Hao, S.; Yan, H.; et al. TLR4 inhibitor resatorvid provides neuroprotection in experimental traumatic brain injury: implication in the treatment of human brain injury. *Neurochem. Int.* **2014**, *75*, 11−8.
(85) Lin, Y.; Luo, T.; Weng, A.; Huang, X.; Yao, Y.; Fu, Z.; et al. Gallic Acid Alleviates Gouty Arthritis by Inhibiting NLRP3 Inflammasome Activation and Pyroptosis Through Enhancing Nrf2 Signaling. *Front Immunol.* **2020**, *11*, No. 580593.
(86) Li, J.; Zhang, G.; Zhi, F.; Zhai, Y.; Zhou, D.; Chen, H.; et al. BtpB inhibits innate inflammatory responses in goat alveolar macrophages through the TLR/NF-κB pathway and NLRP3 inflammasome during Brucella infection. *Microb Pathog.* **2022**, *166*, No. 105536.
(87) Abdel Baky, N. A.; Al-Najjar, A. H.; Elariny, H. A.; Sallam, A. S.; Mohammed, A. A. Pramipexole and Lactoferrin ameliorate Cyclophosphamide-Induced haemorrhagic cystitis via targeting Sphk1/S1P/MAPK, TLR-4/NF-κB, and NLRP3/caspase-1/IL-1β signalling pathways and modulating the Nrf2/HO-1 pathway. *Int. Immunopharmacol.* **2022**, *112*, No. 109282.
(88) Xue, Z., Sun, X., Li, H., Iqbal, M., Qi, L., Wang, F., et al. Composite coatings of S-HA nanoparticles and Schiff base on ZE21B alloy for stronger corrosion resistance and biological performance. *J. Magnesium Alloys* **2024**. DOI: 10.1016/j.jma.2023.11.009
(89) Ge, G.; Bai, J.; Wang, Q.; Liang, X.; Tao, H.; Chen, H.; et al. Punicalagin ameliorates collagen-induced arthritis by downregulating M1 macrophage and pyroptosis via NF-κB signaling pathway. *Sci. China Life Sci.* **2022**, *65* (3), 588−603.
(90) Li, H.; Liang, X.; Chen, Y.; Liu, K.; Fu, X.; Zhang, C.; et al. Synergy of antioxidant and M2 polarization in polyphenol-modified konjac glucomannan dressing for remodeling wound healing microenvironment. *Bioeng. Transl. Med.* **2023**, *8* (2), No. e10398.
(91) Wang, Y.; Huang, S.; Kong, W.; Wu, C.; Zeng, T.; Xie, S.; et al. Corilagin alleviates liver fibrosis in zebrafish and mice by repressing IDO1-mediated M2 macrophage repolarization. *Phytomedicine.* **2023**, *119*, No. 155016.
(92) Li, W.; Yue, X.; Li, F. Gallic acid caused cultured mice TM4 Sertoli cells apoptosis and necrosis. *Asian-Australas J. Anim Sci.* **2019**, *32* (5), 629−36.
(93) Hsieh, S. C.; Wu, C. C.; Hsu, S. L.; Yen, J. H. Molecular mechanisms of gallic acid-induced growth inhibition, apoptosis, and necrosis in hypertrophic scar fibroblasts. *Life Sci.* **2017**, *179*, 130−8.
(94) Bertheloot, D.; Latz, E.; Franklin, B. S. Necroptosis, pyroptosis and apoptosis: an intricate game of cell death. *Cell Mol. Immunol.* **2021**, *18* (5), 1106−21.
(95) Frank, D.; Vince, J. E. Pyroptosis versus necroptosis: similarities, differences, and crosstalk. *Cell Death Differ.* **2019**, *26* (1), 99−114.
(96) Kang, T. B.; Yang, S. H.; Toth, B.; Kovalenko, A.; Wallach, D. Caspase-8 blocks kinase RIPK3-mediated activation of the NLRP3 inflammasome. *Immunity.* **2013**, *38* (1), 27−40.
(97) Jorgensen, I.; Zhang, Y.; Krantz, B. A.; Miao, E. A. Pyroptosis triggers pore-induced intracellular traps (PITs) that capture bacteria and lead to their clearance by efferocytosis. *J. Exp Med.* **2016**, *213* (10), 2113−28.
(98) Hoshyar, N.; Gray, S.; Han, H.; Bao, G. The effect of nanoparticle size on in vivo pharmacokinetics and cellular interaction. *Nanomedicine (Lond).* **2016**, *11* (6), 673−92.
(99) Skotland, T.; Iversen, T. G.; Llorente, A.; Sandvig, K. Biodistribution, pharmacokinetics and excretion studies of intravenously injected nanoparticles and extracellular vesicles: Possibilities and challenges. *Adv. Drug Deliv Rev.* **2022**, *186*, No. 114326.
(100) Choi, C. H.; Zuckerman, J. E.; Webster, P.; Davis, M. E. Targeting kidney mesangium by nanoparticles of defined size. *Proc. Natl. Acad. Sci. U. S. A.* **2011**, *108* (16), 6656−61.
(101) Li, X.; Meng, L.; Zhang, Y.; Qin, Z.; Meng, L.; Li, C.; et al. Research and Application of Polypropylene Carbonate Composite Materials: A Review. *Polymers* **2022**, *14* (11), 2159 DOI: 10.3390/polym14112159.
(102) Dilliard, S. A.; Cheng, Q.; Siegwart, D. J. On the mechanism of tissue-specific mRNA delivery by selective organ targeting nanoparticles. *Proc. Natl. Acad. Sci. U. S. A.* **2021**, *118* (52), No. e2109256118, DOI: 10.1073/pnas.210925611.